2015

$La_{0.6}Sr_{1.4}MnO_{4+\delta}$ Layered Perovskite Oxide: Enhanced catalytic Activity for the Oxygen Reduction Reaction

Yarong Wang

Zhibin Yang

Fanliang Liu

Chao Jin

Jiao Wu

See next page for additional authors

Publication Info

Published in *RSC Advances*, Volume 51, Issue 2, 2015, pages 974-980.

This article was first published by the Royal Society of Chemistry and can be found at http://dx.doi.org/10.1039/C4RA11588K
Wang, Y., Yang, Z., Lu, F., Jin, C., Wu, J., Shen, M., Yang, R., & Chen, F. (2015). Carbon-Coating Functionalized $La_{0.6}Sr_{1.4}MnO_{4+\delta}$ Layered Perovskite Oxide: Enhanced catalytic Activity for the Oxygen Reduction Reaction. RSC Advances, 5 (2), 974 – 980. http://dx.doi.org/10.1039/C4RA11588K

Author(s)
Yarong Wang, Zhibin Yang, Fanliang Liu, Chao Jin, Jiao Wu, Ming Shen, Ruizhi Yang, and Fanglin Chen

RSC Advances

PAPER

View Article Online
View Journal | View Issue

CrossMark click for updates

Cite this: *RSC Adv.*, 2015, **5**, 974

Carbon-coating functionalized $La_{0.6}Sr_{1.4}MnO_{4+\delta}$ layered perovskite oxide: enhanced catalytic activity for the oxygen reduction reaction

Yarong Wang,†[a] Zhibin Yang,†[b] Fanliang Lu,[a] Chao Jin,*[a] Jiao Wu,[a] Ming Shen,[c] Ruizhi Yang*[a] and Fanglin Chen*[d]

Received 1st October 2014
Accepted 26th November 2014

DOI: 10.1039/c4ra11588k

www.rsc.org/advances

Efficient electrocatalysts for the oxygen reduction reaction (ORR) is a critical factor to influence the performance of lithium–oxygen batteries. In this study, $La_{0.6}Sr_{1.4}MnO_{4+\delta}$ layered perovskite oxide as a highly active electrocatalyst for the ORR has been prepared, and a carbon-coating layer with thickness <5 nm has been successfully introduced to enhance the electronic conductivity of the as-prepared oxide. XRD, XPS, Raman, SEM and TEM measurements were carried out to characterize the crystalline structure and morphology of these samples. Rotating ring-disk electrode (RRDE) technique has been used to study catalytic activities of the as-prepared catalysts for the ORR in 0.1 M KOH media. RRDE results reveal that carbon-coated $La_{0.6}Sr_{1.4}MnO_{4+\delta}$ exhibits better catalytic activity for the ORR. For the carbon-coated $La_{0.6}Sr_{1.4}MnO_{4+\delta}$, the ORR proceeds predominately *via* a direct four electron process, and a maximum cathodic current density of 6.70 mA cm^{-2} at 2500 rpm has been obtained, which is close to that of commercial Pt/C electrocatalyst under the same testing conditions.

1. Introduction

In recent years, rechargeable lithium–oxygen batteries have been attracting more and more attention due to higher theoretical energy densities (5200 Wh kg^{-1}, including oxygen) than state-of-the-art lithium ion batteries. The lithium–oxygen battery will enable electric vehicles with driving ranges similar to those of gasoline-powered vehicles if successfully developed.[1–3] Sluggish oxygen reduction reaction (ORR) at air electrode plays a vital role in the optimization of lithium–oxygen batteries. The exploration of efficient electrocatalysts for the ORR is highly necessary for the developing of the lithium–oxygen battery.[4–9] Platinum-based materials have long been regarded as active and efficient catalysts for the ORR. However, the high price, limited storage, sluggish ORR process, and instability of platinum-based catalysts have greatly impeded the commercialization of metal–air batteries.[10–12] Therefore, it is vital and urgent to explore highly efficient non-platinum catalysts for ORR in the air electrode. In recent years, mixed valence oxides of transition metals have attracted much attention because of their prominent advantages of abundance, low cost, environment-friendly, and considerable catalytic activity towards electrochemical ORR.

Among various types of metal oxides, perovskite oxides exhibit good cation ordering, which can provide disorder-free channels of oxygen vacancies to enhance the mobility of oxygen ions.[13,14] Perovskite oxides have long been considered a promising material capable of catalyzing oxygen reduction in metal–air batteries with aqueous alkaline electrolytes.[15–19] For example, $La_{0.6}Ca_{0.4}CoO_3$ perovskite oxide demonstrated promising performances as ORR catalyst for Zn–air battery in 9 M KOH solution.[15] Over several years, some perovskite cathode materials of solid oxide fuel cells (SOFCs) have successively been reported as cathodic catalysts in lithium–oxygen batteries. Yang *et al.* prepared the $Sr_{0.95}Ce_{0.05}CoO_3$ perovskite catalysts loaded with copper nanoparticles and demonstrated improved round-trip efficiency in rechargeable Li–air batteries.[16] Zhao *et al.* synthesized hierarchical mesoporous perovskite $La_{0.5}Sr_{0.5}CoO_{2.91}$ nanowires and used it as cathodic catalyst in lithium–oxygen batteries, which exhibited ultrahigh capacity over 11 000 mA h g^{-1}.[17] As one of the most frequently-used cathode materials of SOFCs, $La_{0.8}Sr_{0.2}MnO_3$ perovskite oxide has also demonstrated promising catalytic properties in Li–air battery with non-aqueous electrolyte in many groups' works.[18,19] As mentioned above, the investigations into perovskite-type catalysts for lithium–oxygen batteries to date have mainly focused on ABO_3 cubic perovskite oxides, where A is main a rare earth metal and B is a transition metal.

[a]*College of Physics, Optoelectronics and Energy & Collaborative Innovation Center of Suzhou Nano Science and Technology, Soochow University, Suzhou 215006, China. E-mail: jinchao@suda.edu.cn; yangrz@suda.edu.cn; chenfa@cec.sc.edu; Tel: +86-512-65221519*

[b]*Union Research Center of Fuel Cell, School of Chemical & Environment Engineering, China University of Mining & Technology, Beijing, 100083, China*

[c]*Huasheng Chemical Corporation, Zhangjiagang, Jiangsu 215635, China*

[d]*Department of Mechanical Engineering, University of South Carolina, Columbia, SC 29208, USA*

† These authors contributed equally to this work.

In our previous reports, some "layered" perovskite oxides ($A_2BO_{4+\delta}$) with K_2NiF_4-type structure demonstrated higher oxygen ionic-transport properties and better electrocatalysis than that of traditional ABO_3 perovskite oxides, and have been successfully applied as electrode materials of SOFCs.[20–22] A recent experimental study suggested that easily removable oxygen in doped La_2NiO_4 "layered" perovskite facilitates the redox reaction of the transition metal, thereby leading to enhanced ORR activity.[23] Unlike a simple perovskite, an $A_2BO_{4+\delta}$ layered perovskite can be described as stacked perovskite (ABO_3) layer alternating with rock-salt (AO) layers along the *c* direction (Fig. 1(a)). Because of the difference in A–O and B–O bond lengths, there is stress in the $A_2BO_{4+\delta}$ structure. Theoretically, it is an unstable structure. In order to eliminate this stress and maintain the structural stability, there are always interstitial oxygen between the ABO_3 perovskite layers and the AO rock-salt layers.[20] In the $A_2BO_{4+\delta}$ materials, oxygen transport occurs *via* a complex mechanism combining interstitial migration in the rock-salt layers and vacancy migration in the perovskite planes, which endows $A_2BO_{4+\delta}$ materials of high oxygen ionic-transport properties and good electrocatalysis.[22] However, electronic conductivity of $A_2BO_{4+\delta}$ layered perovskite is intrinsically poor because AO rock-salt layers could be considered to be an insulator, which limits its high-rate capability even if it could be used in lithium–oxygen batteries. Though doping of aliovalent cations onto $A_2BO_{4+\delta}$ could control lattice defect (B^{3+} and oxygen vacancy) and thus modify its electronic conductivity, this way cannot significantly improve electronic conductivity due to AO rock-salt layers.[23] Surface coating with electronically conductive layers is an extraordinary effective way to enhance the electronic conductivity of $A_2BO_{4+\delta}$ material. Cu, Ag, carbon, and conducting polymers are currently utilized as electronic conducting coating materials.[24,25] Among them, carbon coating is particularly attractive due to its high conductivity, electrochemical stability, low cost, and simplicity of implementation. In addition, intrinsic interconnection between carbon coating layers if also very effective to reduce the contact resistance between active material particles.[26–28] On the other hand, the graphitic carbon coating layer need to be very thin (<5 nm) to allow easy and rapid penetration of oxygen ions. So, it is very challenging to develop an effective approach to produce ultrathin and uniform graphitic carbon coatings.

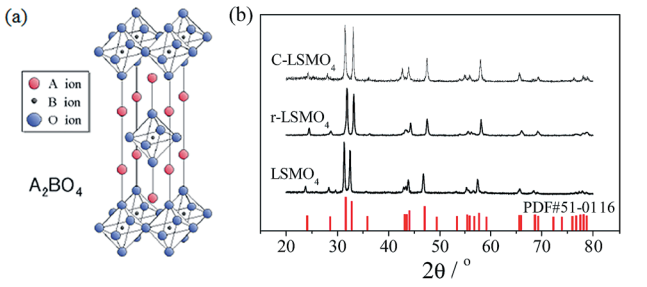

Fig. 1 Crystal structure of an A_2BO_4 layered perovskite (a); XRD pattern of the as-prepared $LSMO_4$, r-$LSMO_4$, C-$LSMO_4$, respectively (b).

Herein, we report a bottom-up strategy to synthesize a carbon-coated $La_{0.6}Sr_{1.4}MnO_{4+\delta}$ composite (C-$LSMO_4$) through a pyrolysis and graphitization process. Sucrose was employed as carbon sources. Graphited carbon-coating was grown on the $LSMO_4$ surface through the realignment of carbon fragments aroused from the pyrolysis of sucrose. The carbon coating is compact and uniform along $LSMO_4$ surface. The electrochemical performance for the ORR of $LSMO_4$ perovskite oxide is remarkably improved with the assistance of carbon coating. To the best of our knowledge, we demonstrate for the first time that carbon-coated $LSMO_4$ catalysts exhibit excellent catalytic performance for the ORR.

2. Experimental section

2.1 Synthesis and preparation

All reagents were analytical grade chemicals and purchased from Guoyao Chemical Reagent Co. Ltd. $La_{0.6}Sr_{1.4}MnO_{4+\delta}$ ($LSMO_4$) powders were prepared through a citric acid–nitrate process as reported.[22] First, $La(NO_3)_3{\cdot}6H_2O$, $Sr(NO_3)_2$, and $Mn(NO_3)_2$ were mixed and dissolved in deionized water according to the stoichiometric compositions of $LSMO_4$; then a certain amount of citric acid was introduced, and the mole ratio of the total metal ion: citric acid was controlled around 1 : 1.5. NH_4OH was added to adjust the pH value to about 8.0. A brown gel was obtained after the solution was agitated over night at 80 °C. This gel was held at 250 °C for several hours to remove organics and form a powder precursor. Finally, the $LSMO_4$ powder was obtained after being calcined at 1000 °C for 8 h.

Preparation of the C-$LSMO_4$ sample was performed as follows: the obtained $LSMO_4$ powder was added into a certain amount of sucrose solution, the mass ratio was controlled at 8 : 1 between $LSMO_4$ and sucrose. The mixtures were heated with vigorous stirring till water was completely evaporated. The mixed powder was grinded and calcined at 900 °C for 12 h under Ar/H_2 (95 : 5 by volume ratio) atmosphere to get final C-$LSMO_4$. For comparisons, the as-prepared $LSMO_4$ powders without carbohydrate coatings were also reduced at 900 °C for 12 h under Ar/H_2 atmosphere. The sample was labeled as r-$LSMO_4$.

2.2 Characterization

The crystal phase of the as-prepared samples was characterized by X-ray powder diffraction (XRD, D/MAX-III-B-40KV, Japan, Cu K_α radiation; $\lambda = 0.15418$ nm). The morphologies and microstructures of the as-prepared samples were carried out using scanning electron microscopy (SEM, Hitachi SU8010) and transmission electron microscopy (TEM; TecnaiG220) with an acceleration voltage of 200 kV. Raman spectroscopy was performed on a Jobin Yvon LabRAM HR800 instrument with a 514 nm excitation laser at a power of around 1 mW. X-ray photoelectron spectroscopy (XPS) analysis was performed with a hemispherical analyzer and using a monochromatized Al Kα (1486 eV) achromatic X-ray radiation. Nitrogen adsorption and desorption isotherms were measured at 77 K with BELSORPmini system (BEL Japan).

2.3 Electrochemical measurement

The procedures of electrode preparation and electrochemical tests were similar to our previous work.[29–31] The electrochemical properties were evaluated with the rotating ring-disk electrode (RRDE) technique using a Pine Electrochemical system (AFMSRX rotator, and AFCBP1 bipotentiostat). The electrode layer was prepared on a glassy carbon (GC) disk by coating a layer of ultrasonically mixed C-$LSMO_4$ and acetylene black ink with a C-$LSMO_4$ loading of 0.4013 mg cm^{-2}. For comparison, samples of $LSMO_4$ and r-$LSMO_4$ were also be prepared and tested with the same procedure, respectively.

A conventional three-electrode electrochemical cell was used for all cyclic voltammetry (CV) and RRDE measurements. The ring electrode collection efficiency of this RRDE was measured to be 0.22. The ring potential was set at 0.5 V to induce complete peroxide decomposition as reported elsewhere.[32] Before taking CV measurements, the KOH solution was bubbled with pure N_2 (99.99%) for at least 30 min to remove any dissolved O_2. For ORR measurements, the KOH solution was bubbled with pure O_2 (99.99%) over 30 min.

3. Results and discussion

3.1 Crystalline phase and microstructure characterization

Fig. 1(b) presents the XRD patterns of pristine $LSMO_4$, reduced $LSMO_4$ (r-$LSMO_4$) and carbon-coated $LSMO_4$ (C-$LSMO_4$). Compared with the standard PDF card, all the diffraction peaks can be well indexed as K_2NiF_4 tetragonal structure with the space group *I4/mmm*, except that a trace peak around 30° corresponding to $La(OH)_3$ and/or La_2O_3 for the pristine $LSMO_4$.[22] The pattern peaks of r-$LSMO_4$ and C-$LSMO_4$ shifted gradually to the high angle direction corresponding to the lattice shrinkage, which roots in the loss of interstitial oxygen during the reducing process. Aguadero and co-authors reported that the lattice expansion phenomenon will happen if there is too much interstitial oxygen in layered perovskite oxide. Conversely, the lattice shrinkage will appear with the loss of interstitial oxygen.[33] Because carbon coating layer could block the interstitial oxygen losing, to some degree, the shift difference of C-$LSMO_4$ is smaller than that of r-$LSMO_4$.

To further confirm XRD results, X-ray photoelectron spectroscopy (XPS) test was performed. As expected, the XPS survey spectrum given in Fig. 2(a) shows the La3d, Sr3d, Mn2p, O1s and C1s peaks for the C-$LSMO_4$ sample. For comparison, Mn2p spectra for pristine $LSMO_4$, r-$LSMO_4$ and C-$LSMO_4$ are also presented in Fig. 2(b)–(d), respectively. It can be seen that Mn–O binding energy increased with the difference of lattice shrinkage after reducing under Ar/H_2 atmosphere. This is consistent with the XRD results.

Raman microprobe spectroscopy was employed to character carbon coating layer. Raman spectra of r-$LSMO_4$, pure acetylene black after calcined at 900 °C for 12 h under Ar/H_2 atmosphere (named as pure C) and C-$LSMO_4$ are shown in Fig. 3, respectively. It can be clearly seen that there is no peaks for r-$LSMO_4$. While, the two intense broad bands at 1345 and 1570 cm^{-1} for pure C and C-$LSMO_4$ are attributed to the D and G bands of

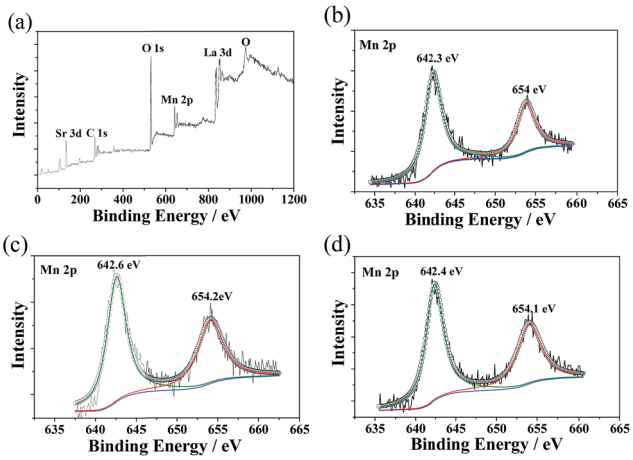

Fig. 2 Full XPS spectra of the as-prepared C-$LSMO_4$ (a); XPS spectra of Mn2p of the as-prepared $LSMO_4$ (b), r-$LSMO_4$ (c) and C-$LSMO_4$ (d), respectively.

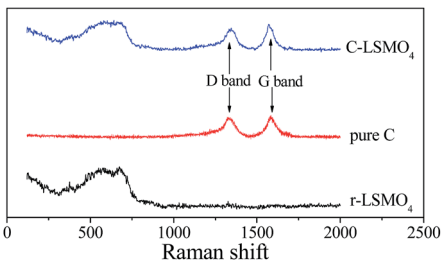

Fig. 3 Raman spectroscopy for r-$LSMO_4$, C-$LSMO_4$ and pure C after calcined at 900 °C for 12 h under Ar/H_2 atmosphere.

carbon. The I_D/I_G ratio is associated with graphitization degree of various carbon materials, the smaller I_D/I_G ratio, the higher graphitization degree.[34,35] The I_D/I_G value for the pure C is 0.94, while that for the C-$LSMO_4$ is 0.85, suggesting a relatively high graphitization degree of carbon-coating layer on the $LSMO_4$ surface.

Fig. 4(a)–(c) display SEM images of pristine $LSMO_4$, r-$LSMO_4$ and C-$LSMO_4$, respectively. Clearly, the as-prepared $LSMO_4$ (see Fig. 4(a)) was well dispersed nanoparticles with the size of 100–200 nm, and the powder was porous, which has relative high specific surface area and is generally accepted microstructure for the ORR. As shown in Fig. 4(b), the r-$LSMO_4$ without the protection of sucrose shows serious agglomeration after calcined at 900 °C for 12 h under Ar/H_2 atmosphere. By comparison, the C-$LSMO_4$ particle (Fig. 4(c)) well maintained their original morphology and size. The phenomenon can be interpreted that carbon-coating layer cut off interconnection of $LSMO_4$ particles and suppressed their agglomeration during sintering. So, we can say that carbon-coating layer not only enhances the electronic conductivity of $LSMO_4$, but also keeps the particle size for short oxygen ion transport pathway.

Carbon morphology and distribution greatly affect the catalytic behavior of as-prepared C-$LSMO_4$ sample. This is because full carbon coverage facilitates electron transfer along

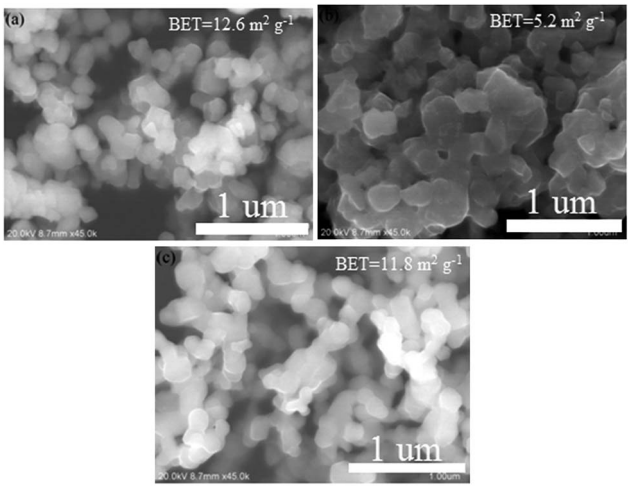

Fig. 4 SEM images of pristine $LSMO_4$ (a), r-$LSMO_4$ (b), and C-$LSMO_4$ (c), respectively.

all directions of the C-$LSMO_4$ particles during electrochemical processes. TEM images of the primary C-$LSMO_4$ particle are presented in Fig. 5. As shown in Fig. 5(a), well dispersed $LSMO_4$ nano-particles with average size of 150 nm is clearly observed, which is in agreement with the SEM result of as-prepared $LSMO_4$. Carbon-coating efficiently hindered $LSMO_4$ particles agglomeration, which is in agreement with the SEM observations. From Fig. 5(b), we can clearly see that carbon-coating layer is uniformly coated the surface of $LSMO_4$ with a thickness of 4.6 nm about. Fig. 5(c) displays detailed structure information of the as-prepared C-$LSMO_4$ by using high-resolution TEM. The measured d spacing of 0.28 nm in the centre of the particle is assigned to the lattice spacing of the (103) plane of $LSMO_4$ perovskite oxide.

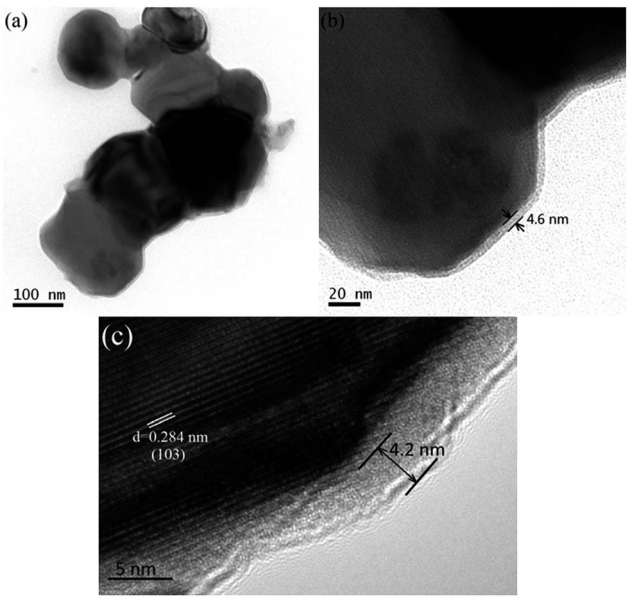

Fig. 5 TEM images of C-$LSMO_4$ with different magnifications, 100 nm bar (a), 20 nm bar (b) and 5 nm bar (c), respectively.

3.2 ORR properties of C-$LSMO_4$

Fig. 6(a) show cyclic voltammetry (CV) scanning results of the as-prepared C-$LSMO_4$ catalyst in O_2 or N_2 saturated 0.1 M KOH solutions, respectively. The C-$LSMO_4$ catalyst displayed an exceptional ORR catalytic activity with an onset potential of *ca.* −0.12 V (*vs.* Ag/AgCl) and one reduction peaks at *ca.* −0.30 V (*vs.* Ag/AgCl).

To better understand the electrocatalytic performance and to evaluate the oxygen reduction kinetic parameters of the C-$LSMO_4$ catalyst during the ORR process, rotating-ring-disk-electrode (RRDE) technique was performed. The measurements were carried out in a cathodic sweep with 10 mV s^{-1} at various rotation speeds (ω) from 400 to 2500 rpm. Fig. 6(b) shows both ring current density (i_r) and disk current density (i_d) of the as-prepared C-$LSMO_4$ catalyst recorded in O_2 saturated 0.1 M KOH solution. From i_d curves, it can be seen that the diffusion limiting current densities increased as rotation speed increase from 400 to 2500 rpm. High rotation speeds lead to faster oxygen flux to electrodes surface and consequently larger currents. The transferred electrons number and the formation of peroxide species (OH_2^-) involved in the ORR are two important parameters to verify the ORR catalytic pathway of the catalyst. The RRDE experiment involves holding the disk at potential E_d, where the reaction $O + ne \rightarrow R$ produces a cathodic current i_d; the ring is kept at a sufficiently positive potential E_r (0.5 V), so that any R reaching the ring is rapidly oxidized.[32] The ring current, i_r, is related to the disk current, i_d, by a quantity N, the capture coefficient. So the transferred electron number (n) and the contents of peroxide HO_2^- during the ORR could be calculated, according to the eqn (1) and (2),[36,37] respectively, as follows:

$$n = 4\frac{i_d}{i_d + (i_r/N)} \quad (1)$$

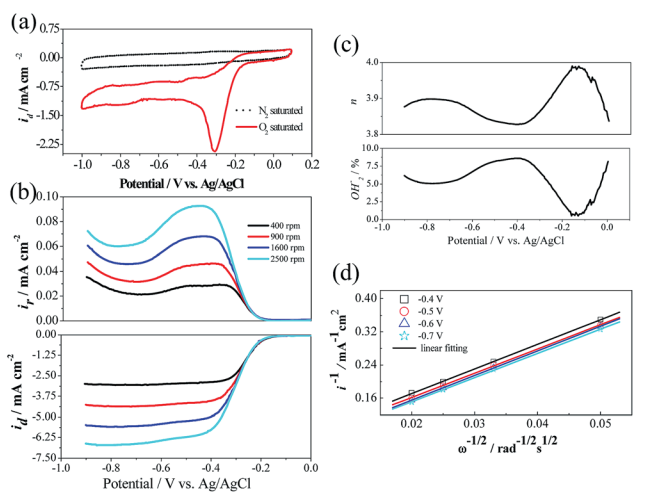

Fig. 6 CV curves of the as-prepared C-$LSMO_4$ catalyst on a GC electrode in N_2 (black dotted curve) and O_2 (red curve) saturated 0.1 M KOH solution at room temperature (a); disk (i_d) and ring (i_r) current densities collected on BCFN electrode for the ORR (b); electron transfer number (n) and peroxide HO_2^- calculated with i_d and i_r (c); Koutecky–Levich plots (d).

$$HO_2^-\% = 100 \times \frac{2i_r/N}{i_d + (i_r/N)} \quad (2)$$

where n is the transferred electron number during the ORR process, i_d is the disk current, i_r is the ring current, and N is the capture coefficient (here, $N = 0.22$).

Fig. 6(c) displays the transferred electron number and the contents of peroxide HO_2^- during the ORR at 2500 rpm. The n values are 3.8–4.0 and the measured HO_2^- yields are below 8.0% over the measured potential range, indicating a $4e^-$ pathway for the C-$LSMO_4$ catalyst during the ORR process.

The Koutecky–Levich plot was used to further characterize the ORR mechanism. According to i_d curves shown in Fig. 6(b), the K–L plots were calculated and displayed in Fig. 6(d) respectively, by using the following equations:[5,38]

$$\frac{1}{i_d} = \frac{1}{i_k} + \frac{1}{i_{dl}} \quad (3)$$

$$i_k = nFAkC_{O_2} \quad (4)$$

$$i_{dl} = 0.62nFC_{O_2}D_{O_2}^{2/3}\nu^{-1/6}\omega^{1/2} = B\omega^{1/2} \quad (5)$$

$$\frac{1}{i_d} = \frac{1}{i_k} + \frac{1}{i_{dl}} = \frac{1}{i_k} + \frac{1}{B}\omega^{-1/2} \quad (6)$$

where i_d, i_k and i_{dl} are the tested disk current density, kinetic current density, and film diffusion limiting current density, respectively. B is the so-called "B-factor". Furthermore, n is the number of electrons in the ORR, F is the Faraday constant (96 500 C mol^{-1}), A is the area of the disk electrode (0.196 cm^{-2}), C_{O_2} is the oxygen concentration in 0.1 M KOH (1.14×10^{-6} mol cm^{-3}), D_{O_2} is the oxygen diffusion coefficient in 0.1 M KOH (1.73×10^{-5} cm^2 s^{-1}), ν is the kinematic viscosity of the 0.1 M KOH solution (0.01 cm^2 s^{-1}), ω is the electrode rotation rate (rpm), k is the rate constant for the ORR. There should be a linear relationship between i_d^{-1} and $\omega^{-1/2}$, the intercept is equal to i_k^{-1}, and the number of the electron transferred during the reaction could be calculated from the slope.[5,29–31]

From Fig. 6(d), it can be seen that all fitting plots appear well linear and parallel relationship, implying the first-order dependence of the ORR kinetics on the C-$LSMO_4$ catalyst surface. Each straight line intercept corresponds to the kinetic current i_k. According to the slop of K–L plots, the "B-factor" was determined with a value of 0.146 mA cm^{-2} $\omega^{-1/2}$, and the electron number was further calculated with a value of 3.86. The result was also indicated a $4e^-$ pathway for the C-$LSMO_4$ catalyst during the ORR process.

3.3 Comparison of ORR catalytic activities

To better understand the electrocatalytic performance of the C-$LSMO_4$ catalyst during the ORR process, the comparison between the ORR activities on $LSMO_4$, r-$LSMO_4$ and pure C as measured with the RRDE is shown in Fig. 7. The ORR activity on commercial Pt/C (20 wt% Pt on carbon) is also included for comparison. The disk and ring currents were measured at 2500 rpm and normalized by the geometric surface area. According to the results shown in Fig. 7, the onset potential, half-wave potential and diffusion limiting current density of these five catalysts were displayed in Table 1. The ORR activity increase as follows: C < $LSMO_4$ < r-$LSMO_4$ < C-$LSMO_4$ < Pt/C, as evidenced by these three parameters shown in Table 1. The diffusion limiting current density of −6.70 mA cm^{-2} for the C-$LSMO_4$ was obtained, which is near to that of Pt/C (−7.14 mA cm^{-2}), and a half-wave potential difference of about 137 mV exists between C-$LSMO_4$ and Pt/C. Considering our tested diffusion limiting current density and half-wave potential of the Pt/C are in good agreement with the values of Pt/C (20 wt% Pt) reported elsewhere,[37,39] we can conclude that C-$LSMO_4$ is more active and comparable to the activity of Pt/C. Fig. 8 shows the transferred electron number of these catalysts. The electron transfer number of 3.85–4.0 for C-$LSMO_4$ was more comparable to that of Pt/C catalyst.

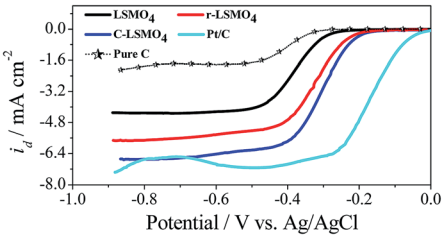

Fig. 7 Linear sweeping voltammograms (LSVs) on the rotating ring-disk electrode for pure C, pristine $LSMO_4$, r-$LSMO_4$, C-$LSMO_4$ and commercial Pt/C in O_2 saturated 0.1 M KOH solution at 2500 rpm.

Fig. 9 shows Tafel plots of these four samples. The kinetic currents were derived from the mass-transport correction using eqn (6) to construct the Tafel plots. It can be observed that the smallest Tafel slope of 62 mV dec^{-1} was obtained for the C-$LSMO_4$ at low overpotentials, which is close to the theoretical value of $2.303RT/F$ (*i.e.*, 59 mV dec^{-1} at 25 °C), where R is the universal gas constant, F is the Faraday constant, and T is the absolute temperature. The lower Tafel slope indicates the high intrinsic catalytic activity of C-$LSMO_4$.

Oxygen species were analyzed by XPS to interpret electrochemical performances of three $LSMO_4$ catalysts. Fig. 10(a)–(c) display O1s XPS spectra of $LSMO_4$, r-$LSMO_4$ and C-$LSMO_4$, respectively. The signal at BE = *ca.* 530 eV is attributed to lattice oxygen (O_2^{2-}) and the one at BE = *ca.* 531 eV to surface adsorbed oxygen species (such as O^-, O_2^- or O_2).[40,41] The lattice oxygen includes bulk lattice oxygen and interstial oxygen. Here, both of bulk lattice oxygen and interstial oxygen are contained

Table 1 Summary of the ORR Catalytic characteristics of pristine $LSMO_4$, r-$LSMO_4$, C-$LSMO_4$, Pt/C and pure C

Catalyst	Onset potential (V *vs.* Ag/AgCl)	Half-wave potential (V *vs.* Ag/AgCl)	i_d (mA cm^{-2})
$LSMO_4$	−0.240	−0.383	−4.28
r-$LSMO_4$	−0.172	−0.323	−5.72
$LSMO_4$	−0.149	−0.306	−6.70
Pt/C	0.003	−0.169	−7.14
Pure C	−0.284	−0.401	−1.82

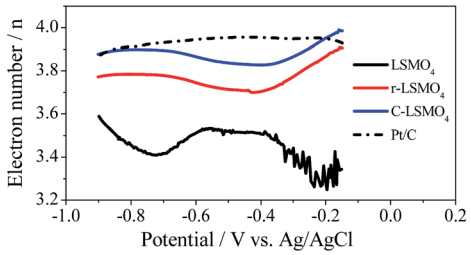

Fig. 8 Comparison of electron transfer number of pristine $LSMO_4$, r-$LSMO_4$, C-$LSMO_4$ and commercial Pt/C calculated with i_d and i_r.

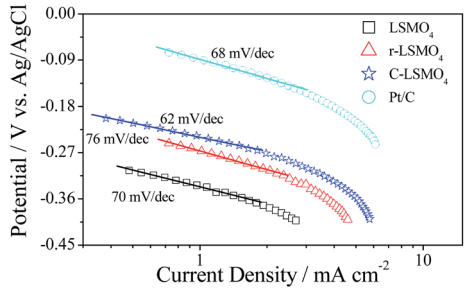

Fig. 9 Tafel plots of pristine $LSMO_4$, r-$LSMO_4$, C-$LSMO_4$ and commercial Pt/C derived by the mass transport correction of corresponding LSV data recorded in O_2 saturated 0.1 M KOH at 2500 rpm.

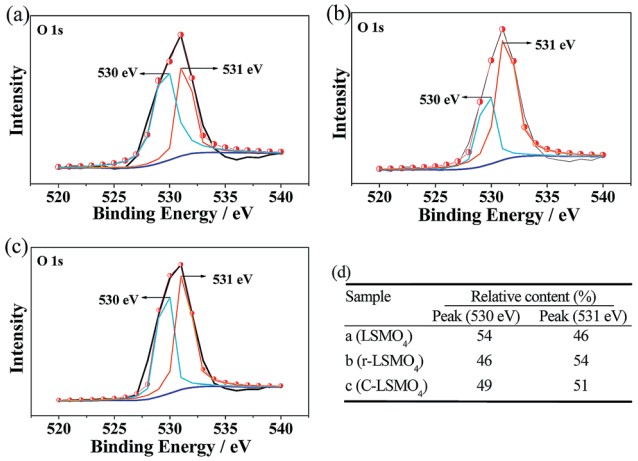

Fig. 10 XPS spectra of O1s of the as-prepared $LSMO_4$ (a), r-$LSMO_4$ (b) and C-$LSMO_4$ (c), respectively; relative contents of different oxygen species in these three samples (d).

in $A_2BO_{4+\delta}$ layered perovskite oxides, and the interstial oxygen is preferentially to be lost during the reducing process. Furthermore, the lattice oxygen is often more active than the surface oxygen.[42] Therefore, the over interstial oxygen will transfer to adsorbed oxygen during the reducing process of $LSMO_4$. Fig. 10(d) shows relative contents of different oxygen species in these three samples. According to the order of $LSMO_4$, C-$LSMO_4$ and r-$LSMO_4$, it can be concluded that the content of lattice oxygen reduced, while that of adsorbed oxygen species increased. In alkaline media, several factors would be concerned for the ORR, such as O_2 adsorption, HO_2^- decomposition, as well as ionic and electronic transportation.[37] After reduced by Ar/H_2 at high temperature, lattice oxygen number decreased, and there would contain more defects, which are beneficial to surface adsorption of O_2 and dissociation of O–O bonds. As a result, reducing treated $LSMO_4$ (r-$LSMO_4$ and C-$LSMO_4$) should exhibit better catalytic performance than that of pristine $LSMO_4$. As for the comparison between r-$LSMO_4$ and C-$LSMO_4$, there are two other rationalized reasons which determine better catalytic performance of C-$LSMO_4$. First, electrical conductivity plays an important role in affecting the catalytic activity of perovsikite oxide. Carbon coating enhances the electrical conductivity by one or two orders of magnitude, which should greatly favor fast electronic transfer and reduce electrode polarization during the catalytic ORR process; second, C-$LSMO_4$ is more porous and has higher surface area than r-$LSMO_4$ as shown in Fig. 4(b) and (c). Higher surface areas permit more active sites for the contact between catalyst and electrolyte. More porous microstructure might facilitate the diffusion, adsorption, and transport of O_2 gas. Therefore, the superiority of C-$LSMO_4$ is understandable.

4. Conclusions

In conclusion, $La_{0.6}Sr_{1.4}MnO_{4+\delta}$ layered perovskite oxide has been synthesized and introduced as catalyst for oxygen reduction reaction. To enhance electronic conductivity of $La_{0.6}Sr_{1.4}MnO_{4+\delta}$ oxide, a surface carbon coating with thickness of <5.0 nm has successfully prepared. Carbon-coating layer not only enhances the electronic conductivity of the material, but also keeps the particle size for short distance of oxygen ion transport. Electrochemical investigations reveal that $La_{0.6}Sr_{1.4}MnO_{4+\delta}$ with carbon coating showed high activities for the ORR in alkaline media, which is comparable to those of commercial Pt/C catalyst.

Acknowledgements

The project was supported by National Natural Science Foundation of China (51272167, 21206101), Natural Science Foundation of Jiangsu Province, China (BK20141199), Natural Science Foundation of the Higher Education Institutions of Jiangsu Province, China (12KJB430010, 14KJB480005). F. Chen acknowledges the financial support from the HeteroFoaM Center, an Energy Frontier Research Center funded by the U.S. Department of Energy, Office of Science, Basic Energy Sciences under Award # DE-SC0001061.

Notes and references

1 M. Armand and J. M. Tarascon, *Nature*, 2008, **451**, 652.
2 G. Girishkumar, B. A. McCloskey, C. Luntz, S. Swanson and W. Wilcke, *J. Phys. Chem. Lett.*, 2010, **1**, 2193.
3 F. Y. Cheng and J. Chen, *Chem. Soc. Rev.*, 2012, **41**, 2172.
4 M. K. Debe, *Nature*, 2012, **486**, 43.
5 Y. Y. Liang, Y. G. Li, H. L. Wang, J. G. Zhou, J. Wang, T. Regier and H. J. Dai, *Nat. Mater.*, 2011, **10**, 780.

6 W. Wang, R. F. Wang, S. Ji and H. Wang, *J. Power Sources*, 2010, **195**, 3498.
7 H. A. Gasteiger, S. S. Kocha, B. Sompalli and F. T. Wagner, *Appl. Catal., B*, 2005, **56**, 9.
8 W. Yang, J. Salim, C. Ma, C. W. Sun, L. Q. Chen and Y. Kim, *Electrochem. Commun.*, 2013, **28**, 13.
9 J. K. Kim, W. Yang, J. Salim, C. W. Sun and Y. Kim, *J. Electrochem. Soc.*, 2014, **161**, A285.
10 Y. Xu, A. V. Ruban and M. Mavrikakis, *J. Am. Chem. Soc.*, 2004, **125**, 4717.
11 C. Wang, H. Daimon, Y. Lee and S. Sun, *J. Am. Chem. Soc.*, 2007, **129**, 6974.
12 Y. Lee, J. Suntivich, K. J. May, E. E. Perry and Y. Shao-Horn, *J. Phys. Chem. Lett.*, 2012, **3**, 399.
13 J. Suntivich, K. J. May, H. A. Gasteiger, J. B. Goodenough and Y. Shao-Horn, *Science*, 2011, **334**, 1183.
14 C. Jin, X. C. Cao, F. L. Lu, Z. R. Yang and R. Z. Yang, *Int. J. Hydrogen Energy*, 2013, **38**, 10389.
15 S. Malkhandi, B. Yang, A. K. Manohar, G. K. Prakash and S. R. Narayanan, *J. Phys. Chem. Lett.*, 2012, **3**, 967.
16 W. Yang, J. Salim, S. Li, C. Sun, C. Chen, J. B. Goodenough and Y. Kim, *J. Mater. Chem.*, 2012, **22**, 18902.
17 Y. L. Zhao, L. Xu, L. Q. Mai and X. Liu, *Proc. Natl. Acad. Sci. U. S. A.*, 2012, **109**, 19569.
18 Z. H. Fu and A. H. Yu, *J. Solid State Electrochem.*, 2012, **16**, 1447.
19 J. J. Xu, D. Xu, Z. L. Wang and X. B. Zhang, *Angew. Chem., Int. Ed.*, 2013, **52**, 3887.
20 C. Jin, J. Liu and J. Sui, *J. Power Sources*, 2008, **182**, 482.
21 C. Jin and J. Liu, *J. Alloys Compd.*, 2009, **474**, 573.
22 C. Jin, Z. B. Yang, H. H. Zheng, C. H. Yang and F. L. Chen, *Electrochem. Commun.*, 2012, **14**, 75.
23 K. N. Jung, J. H. Jung, S. Yoon, K. H. Shin and J. W. Lee, *ACS Appl. Mater. Interfaces*, 2013, **5**, 9902.
24 Y. H. Huang and J. B. Goodenough, *Chem. Mater.*, 2008, **20**, 7237.
25 D. Lepage, C. Michot, G. X. Liang, M. Gauthier and S. B. Schougaard, *Angew. Chem., Int. Ed.*, 2011, **50**, 6884–6887.
26 J. J. Wang and X. L. Sun, *Energy Environ. Sci.*, 2012, **5**, 5163.
27 J. B. Hou, Y. Y. Shao, M. W. Ellis, R. B. Moore and B. L. Yi, *Phys. Chem. Chem. Phys.*, 2011, **13**, 15384.
28 H. Q. Li and H. S. Zhou, *Chem. Commun.*, 2012, **48**, 1201.
29 A. Aguadero, M. Pérez and L. Daza, *J. Power Sources*, 2005, **151**, 52.
30 X. L. Wu, L. Y. Jiang, Y. G. Guo and L. J. Wan, *Adv. Mater.*, 2009, **21**, 2710.
31 J. Li, Q. T. Qu, L. F. Zhang, L. Zhang and H. H. Zheng, *J. Alloys Compd.*, 2013, **579**, 377.
32 T. Hyodo, M. Kayashi, N. Miura and N. Yamazoe, *J. Electrochem. Soc.*, 1996, **143**, L266.
33 F. Y. Cheng, Y. Su, J. Liang, Z. L. Tao and J. Chen, *Chem. Mater.*, 2010, **22**, 898.
34 G. U. Kulkarni, C. R. Rao and M. W. Roberts, *J. Phys. Chem.*, 1995, **99**, 3310.
35 C. Jin, X. C. Cao, L. Y. Zhang, C. Zhang and R. Z. Yang, *J. Power Sources*, 2013, **241**, 225.
36 C. Jin, F. L. Lu, X. C. Cao, Z. R. Yang and R. Z. Yang, *J. Mater. Chem. A*, 2013, **1**, 12170.
37 C. Jin, X. C. Cao and R. Z. Yang, *ACS Appl. Mater. Interfaces*, 2014, **6**, 847.
38 J. Wu, Z. R. Yang, X. W. Li, Q. J. Sun, C. Jin, P. Strasser and R. Z. Yang, *J. Mater. Chem. A*, 2013, **1**, 9889.
39 J. B. Goodenough and A. Manthiram, *J. Solid State Chem.*, 1990, **88**, 115.
40 J. G. Deng, L. Zhang, H. X. Dai and C. T. Au, *Appl. Catal., B*, 2009, **89**, 87.
41 S. B. Adler, *Chem. Rev.*, 2004, **104**, 4791.
42 J. Sunarso, A. A. Torriero, W. Zhou and M. Forsyth, *J. Phys. Chem. C*, 2012, **116**, 5827.